

An approach for identifying sources of inadequacy and upgrades in models with high-dimensional outputs and boundary conditions

Filippo Monari

Mechanical and Aerospace Engineering, University of Strathclyde, Glasgow (UK)

`filippo.monari@strath.ac.uk`

April 5, 2022

Abstract

The construction of computer models (mathematical models implemented in computer codes), with respect to observed phenomena, is usually undertaken by building different variants depending on modeller sensibility, and choosing the one yielding the best fit of the field data, according to Root Mean Squared Error (RMSE) based measures. Usually a particular model is chosen because of its marginally lower RMSE, and not because of its actual higher adequacy, risking that its capability of extrapolating predictions is poor. This work aims at improving the current practice in the creation of computer models by proposing an approach similar to those employed in statistical modelling, wherein starting from the simplest hypothesis, effective model upgrades are identified by analysing discrepancies between observations and predictions, and different model variants are compared according to robust likelihood based criteria. The method, focused on models with high dimensional outputs and boundary conditions and centred on Bayesian calibration, is demonstrated on numerical experiments considering a series of building energy models. The object of the modelling is a test facility used for round robin tests in the context of the International Energy Agency (IEA), Energy Building and Communities (EBC), Annex 58.

1 Introduction

Mathematical models implemented in computer codes (computer models) have reached great capabilities at representing real world phenomena, and nowadays are indispensable for solving many problems related to different fields of engineering. Nonetheless, they are characterised by complex mathematical structures, and their creation requires a significant amount of detailed information (prior information), which is not always available and usually affected by substantial uncertainties. Often, it is necessary to tailor the model structure according to the available prior information and to its embedded uncertainties, by making assumptions, deciding which aspects deserve more focus, and selecting suitable abstractions. It is useful to make an example, connecting with the case study presented later, to better clarify this point. With respect to building energy models, which are perfect examples of complex computer models with many inbuilt integrated components attempting to represent reality, even modelling the simplest building involve choosing among several possibilities,

for example: which materials to assume for the envelop components, whether or not to consider air infiltration, in the latter case whether to adopt a constant infiltration model or a wind driven infiltration model, and whether to use an ideal abstraction for the heating/cooling system rather than a more detailed dedicated model.

With respect to the modelling of observed processes, the development of computer models involves (i) the treatment and reduction of the uncertainties contained within the prior information, and (ii) the assessment of the adequacy of the proposed model structure, that is the adequate consideration of all the processes underpinning a the real phenomenon being modelled. While the former issue has been object of substantial research, resulting in the formulation of methodologies such as Bayesian calibration of which a brief literature review follows, the latter has been rarely investigated [20, 19].

In practice, suitable model structures are defined by assessing the capabilities of matching field data of different variants, built depending on modeller sensibility and expertise, according to metrics based upon the Root Mean Squared Error (RMSE). Because of its discretionary character, the overparametrisation caused by the complex underpinning mathematical structures, and equifinality (i.e. different models yielding very similar RMSE, despite having significantly different characteristics), this approach often fails in selecting the most suitable model of the observed phenomenon. Indeed, a particular model structure is chosen just because of its marginally better RMSE, and not Because of its actual higher adequacy, risking that its capability of extrapolating predictions is poor. This work aims at improving the current practice for the creation of computer models by proposing an approach similar to those employed in statistical modelling, wherein starting from the simplest hypothesis, effective model upgrades are identified by analysing discrepancies between observations and predictions, and different model variant are compared according to likelihood based criteria (e.g. Akaike Information Criterion, Bayes Information Criterion or Likelihood Ratios) resilient to overparameterisation and equifinality. The presented approach focuses on models with high dimensional outputs and boundary conditions, and is centred on Bayesian calibration.

Bayesian calibration is a popular framework used to infer parameter values in computer models. The first mathematical formulation was described in [13]. Building on this formulation, a series of works have demonstrated the capability of Bayesian calibration in a number of different case studies [9, 2, 3]. Subsequently, the representation of high-dimensional model outputs through basis expansions has allowed the application of the Bayesian paradigm to the calibration of a wide range of computer models [7, 1, 8]. Generally Bayesian calibration relies on probabilistic models based on Gaussian Process Regression [18], allowing the Bayesian inference of the computer model parameters (calibration parameters): the simulation model, providing a probabilistic emulator of the computer model, and the observation model, giving a probabilistic depiction of the observed data. The latter in turn is composed of the calibration model, allowing the estimation of the calibration parameters, and the discrepancy model, which represent the difference between model predictions and observations due to inadequacies within the computer model (discrepancy). Identifiability problems may raise due to interference between the discrepancy model, and the calibration model [13, 2]. These issues have been object of recent research, and possible solutions have been proposed in [17, 21].

In the presented approach, as in [20, 19], the identification of deficiencies in the model structure is undertaken through the modelling of the discrepancy between predictions and observations. These studies propose the assessment of the model adequacy, by modelling the discrepancy within the mathematical structure of the model, which is decomposed in a series of sub-functions. Since the mathematical structure of computer models is not usually directly accessible, in this work the

discrepancy is modelled externally by exploiting the discrepancy term included in the Bayesian calibration framework. In particular, a Gaussian process prior probability density distribution that avoids conflicts with the simulation and calibration counterparts is adopted. Its hyper parameters are linked to the boundary conditions and used to quantify their correlation with the discrepancy between predictions and measurements. This information can then be used by the modeller for proposing model upgrades, directly addressing those aspects affected by the boundary conditions with higher correlations. Different models are compared by means of Bayes Factors. The proposed methodology is demonstrated on numerical experiments considering synthetically generated and measured data, which analyse a series of building energy models. The modelling environment is provided by the dynamic simulation program ESP-r [4]. The object of the modelling is a test facility used for round robin tests in the context of the International Energy Agency (IEA), Energy Building and Communities (EBC), Annex 58 (<http://www.iea-ebc.org/projects/completed-projects/ebc-annex-58>). The aim of this international project was to investigate the capability of different methods for characterising thermal properties and features of building envelopes, of which the test box was a simplified, but realistic, surrogate.

2 Method

The addressed problem is the following. A real process, subject to S known time varying boundary conditions ($\mathbf{X} = [\mathbf{x}_1, \dots, \mathbf{x}_s, \dots, \mathbf{x}_S]$), and determined by unknown time independent parameters, is observed by measuring N times a target variable (\mathbf{y}^*). R different models of the observed process, accounting for \mathbf{X} , are available. The r -th model (\mathcal{M}_r) has unknown underlying mathematical structure, and P free parameters ($\mathbf{z} = [z_1, \dots, z_p, \dots, z_P]$) representing the time independent unknowns ($\mathbf{z}^* = [z_1^*, \dots, z_p^*, \dots, z_P^*]$). Having a sample of M \mathbf{z} ($\mathbf{Z} = [\mathbf{z}_1, \dots, \mathbf{z}_m, \dots, \mathbf{z}_M]^T$), \mathcal{M}_k provides a set of predictions for \mathbf{y}^* ($\mathbf{Y} = [\mathbf{y}_1, \dots, \mathbf{y}_m, \dots, \mathbf{y}_M]$). Therefore, it is necessary to: (i) infer the values of the parameters in \mathbf{z}^* (calibration parameters); (ii) learn about causes of discrepancy between predictions and measurements, in order to provide effective model improvements; (iii) effectively select among the R created variants the model providing the best description of the observed process. To solve these problems, the following three steps are undertaken: (i) quasi-Bayesian calibration, (ii) discrepancy analysis, and (iii) model selection. Their explanation follows.

2.1 Quasi-Bayesian calibration

This section describes the mathematical framework used for model calibration, which builds on [8]. However, the involved probabilistic models are explicitly expressed as a factorisation of terms, which are easier to process. The overall framework is quasi-Bayesian, that is the hyper parameters of the simulation model are optimised and fixed afterwards. This approximation is generally accepted since, while giving results similar to a fully Bayesian analysis, it allows a great simplification of the calculation involved [1].

2.1.1 Simulation model

Each simulation output (\mathbf{y}_m) is represented by the sum of the model emulator ($f(\mathbf{z}_m) = \mathbf{K}w(\mathbf{z}_m)$) and white noise ($\varepsilon \sim \mathcal{N}(0, \lambda^{-1})$, with $\lambda \sim \mathcal{Gamma}(a, b)$).

$$\mathbf{y}_m = f(\mathbf{z}_m) + \varepsilon = \mathbf{K}w(\mathbf{z}_m) + \varepsilon \quad (1)$$

where the $N \times Q$ matrix \mathbf{K} has as columns orthogonal vectors (\mathbf{k}_q) defined as explained in Section 2.1.3. The function $w(\cdot)$ can be expressed with Q Gaussian Processes (\mathcal{GP} s), modelling the Q set of coefficients associated with the vectors \mathbf{k}_q :

$$w_q(\mathbf{Z}_q) \sim \mathcal{GP}(\mathbf{0}, \varrho_q(\mathbf{Z}_q, \mathbf{Z}_q, \gamma_q) + \mathbf{I}\lambda_q^{-1}) \quad (2)$$

where γ_q represents the hyper parameters, and $\mathbf{Z}_q = [\mathbf{z}_{q,1}, \dots, \mathbf{z}_{q,m}, \dots, \mathbf{z}_{q,M}]^T$, with $\mathbf{z}_{q,m}$ the vector containing the subset of values of \mathbf{z}_m relative only to the parameters significant for the q -th \mathcal{GP} . In particular these parameters are selected according to the forward selection strategy outlined in [24].

Optimal values of the precision parameters ($\boldsymbol{\lambda} = [\lambda_1, \dots, \lambda_q, \dots, \lambda_Q]$), and of the covariance function hyper parameters ($\boldsymbol{\gamma} = [\gamma_1, \dots, \gamma_q, \dots, \gamma_Q]$), are determined by maximising the corresponding joint probability density distribution conditional on $\mathbf{W} = [\hat{\mathbf{w}}_1, \dots, \hat{\mathbf{w}}_q, \dots, \hat{\mathbf{w}}_Q]$ and \mathbf{Z} :

$$\begin{aligned} p(\boldsymbol{\lambda}, \boldsymbol{\gamma} | \mathbf{W}, \mathbf{Z}) &\propto \\ &\prod_{q=1}^Q [(2\pi)^{-\frac{M}{2}} |\mathbf{I}\lambda_q^{-1} + \varrho_q(\mathbf{Z}_q, \mathbf{Z}_q, \gamma_q)|^{-\frac{1}{2}} \exp\{-\frac{1}{2} \hat{\mathbf{w}}_q^T [\mathbf{I}\lambda_q^{-1} + \varrho_q(\mathbf{Z}_q, \mathbf{Z}_q, \gamma_q)]^{-1} \hat{\mathbf{w}}_q\} \times \\ &\times \frac{(\frac{b'}{\mathbf{k}_q^T \mathbf{k}_q})^{a'}}{\Gamma(a')} \lambda_q^{a'-1} \exp\{-\frac{b'}{\mathbf{k}_q^T \mathbf{k}_q} \lambda_q\} \times p(\gamma_q) \end{aligned} \quad (3)$$

where:

$$\begin{aligned} a' &= a + \frac{M(N-Q)}{2} \\ b' &= b + \frac{1}{2} \sum_{m=1}^M \mathbf{y}_m^T (\mathbf{I} - \mathbf{K}(\mathbf{K}^T \mathbf{K})^{-1} \mathbf{K}^T) \mathbf{y}_m \\ \hat{\mathbf{w}}_q &= (\mathbf{k}_q^T \mathbf{k}_q)^{-1} \mathbf{k}_q^T \mathbf{Y} \end{aligned}$$

The r -th model, probabilistically characterised by the calculated optimal values of the corresponding $\boldsymbol{\gamma}$ and $\boldsymbol{\lambda}$ parameters, is indicated with the symbol \mathcal{M}_r .

2.1.2 Observation model

The model representing the measured observation (\mathbf{y}^*) is composed of: (i) the calibration model, that is the physical model emulator evaluated at the unknown parameter values \mathbf{z}^* ($f(\mathbf{z}^*) = \mathbf{K}w^*(\mathbf{z}^*)$); (ii) the discrepancy model, dependent only on the known variable boundary conditions ($\Delta(\mathbf{X}) = \mathbf{H}v(\mathbf{X})$); and (iii) i.i.d. Gaussian noise ($\boldsymbol{\varepsilon}^* \sim \mathcal{N}(0, \lambda^{*-1})$, with $\lambda^* \sim \mathcal{Gamma}(a^*, b^*)$):

$$\mathbf{y}^* = f(\mathbf{z}^*) + \Delta(\mathbf{X}) + \boldsymbol{\varepsilon}^* = \mathbf{K}w^*(\mathbf{z}^*) + \mathbf{H}v(\mathbf{X}) + \boldsymbol{\varepsilon}^* \quad (4)$$

where \mathbf{H} is an $N \times (N-Q)$ matrix, having as columns orthonormal vectors (\mathbf{h}_d) orthogonal to \mathbf{K} (Section 2.1.3), and $v(\mathbf{X}) \sim \mathcal{GP}(\mathbf{0}, \mathbf{H}^T \zeta(\mathbf{X}) \mathbf{H})$. Thus, \mathbf{y}^* is decomposed according to two models, $f(\mathbf{z}^*)$ and $\Delta(\mathbf{X})$, spanning complementary spaces, defined by \mathbf{K} and \mathbf{H} respectively. The former explains the variance of \mathbf{y}^* lying within the simulation space, while the latter explains the variance of \mathbf{y}^* lying outside (or orthogonal to) such space (i.e. the discrepancy).

The calibration model, is used to estimate the calibration parameters (\mathbf{z}^*), and it is developed as follows. Analogously to Section 2.1.1, the function $w^*(\cdot)$ is expressed by Q \mathcal{GP} s. However, in this case the \mathcal{GP} s are conditioned upon their counterparts in Equation (2):

$$w_q^*(\mathbf{z}_q^*) \sim \mathcal{GP}(w'_q, \sigma_q'^2)$$

where:

$$\begin{aligned} w'_q &= \varrho_q(\mathbf{z}_q^*, \mathbf{Z}_q, \gamma_q)[\varrho_q(\mathbf{Z}_q, \mathbf{Z}_q, \gamma_q) + \mathbf{I}\lambda_q^{-1}]^{-1}\hat{w}_q \\ \sigma_q'^2 &= [\lambda_q^{*-1} + \varrho_q(\mathbf{z}_q^*, \mathbf{z}_q^*, \gamma_q)] - \varrho_q(\mathbf{z}_q^*, \mathbf{Z}_q)[\varrho_q(\mathbf{Z}_q, \mathbf{Z}_q, \gamma_q) + \mathbf{I}\lambda_q^{-1}]^{-1}\varrho_q(\mathbf{Z}_q, \mathbf{z}_q^*, \gamma_q) \end{aligned}$$

Posterior probability density distributions for the calibration ($\mathbf{z}^* = \bigcup\{\forall \mathbf{z}_q : q = 1, \dots, Q\}$) and precision ($\boldsymbol{\lambda}^* = [\lambda_1^*, \dots, \lambda_q^*, \dots, \lambda_Q^*]$) parameters are inferred by integrating with Markov Chain Monte Carlo (MCMC) methods their joint posterior probability density distribution, given $\hat{\mathbf{w}}^* = [\hat{w}_1^*, \dots, \hat{w}_q^*, \dots, \hat{w}_Q^*]$ (where $\hat{w}_q^* = (\mathbf{k}_q^T \mathbf{k}_q)^{-1} \mathbf{k}_q^T \mathbf{y}^*$), and \mathcal{M}_r :

$$p(\mathbf{z}^*, \boldsymbol{\lambda}^* | \hat{\mathbf{w}}^*, \mathcal{M}_r) \propto \prod_{q=1}^Q [(2\pi\sigma_q'^2)^{-\frac{1}{2}} \exp\{-\frac{(\hat{w}_q^* - w'_q)^2}{2\sigma_q'^2}\}] \times \frac{(\frac{b^*}{\mathbf{k}_q^T \mathbf{k}_q})^{a^*} (\lambda_q^*)^{a^*-1}}{\Gamma(a^*)} \exp\{-\frac{b^* \lambda_q^*}{\mathbf{k}_q^T \mathbf{k}_q}\}] \times p(\mathbf{z}^*) \quad (5)$$

$p(\mathbf{z}^*)$ indicates the prior probability density distributions chosen for \mathbf{z}^* .

The discrepancy model ($\Delta(\mathbf{X})$) is used to investigate correlation relationships between boundary conditions and the discrepancy (Section 2.3). Empirical probability density distributions for its unknown hyper parameters and precision parameter λ^* , are estimated by integrating with MCMC algorithms the relative joint posterior probability density distribution given $\hat{\mathbf{v}} = (\mathbf{H}^T \mathbf{H})^{-1} \mathbf{H}^T \mathbf{y}^*$, and \mathbf{X} :

$$\begin{aligned} p(\boldsymbol{\gamma}^*, \lambda^* | \hat{\mathbf{v}}, \mathbf{X}) &\propto \\ (2\pi)^{-\frac{1}{2}} |\mathbf{H}^T (\lambda^{*-1} + \zeta(\mathbf{X}, \mathbf{X})) \mathbf{H}|^{-\frac{1}{2}} \exp\{-\frac{1}{2} \hat{\mathbf{v}}^T [\mathbf{H}^T (\lambda^{*-1} + \zeta(\mathbf{X}, \mathbf{X})) \mathbf{H}]^{-1} \hat{\mathbf{v}}\} \times \\ \frac{(a^{*'})^{b^{*'}}}{\Gamma(a^{*'})} (\lambda^*)^{a^{*'}-1} \exp\{-b^{*'} \lambda^*\} \times p(\mathbf{z}^*) \times p(\boldsymbol{\gamma}^*) \end{aligned} \quad (6)$$

The MCMC method used to integrate Equations (5) and (6) is the Annealed Importance Sampling (AIS) algorithm [16], which allows also the calculation of the respective normalising constants used for performing model selection (Section 2.4).

2.1.3 Basis systems definition

The field observations (\mathbf{y}^*) are decomposed according to the basis systems \mathbf{K} and \mathbf{H} , the former spanning the model simulation space and the latter spanning the complementary space needed to completely explain their variance.

The matrix \mathbf{K} is defined as follows. The first $Q - 1$ columns are a subset of the eigenvectors of the matrix $\mathbf{Y}_c \mathbf{Y}_c^T$ (where \mathbf{Y}_c is the matrix \mathbf{Y} after having centred its columns on zero) scaled by the respective singular values. In particular, these eigenvectors are calculated by Singular Value Decomposition (SVD), and selected according to the relative eigenvalues, so as to explain the 99%

of the total variance contained in \mathbf{Y}_c . The Q -th column of \mathbf{K} is the vector composed of all ones, so that $\hat{\mathbf{w}}_Q$ corresponds to the subtracted simulation mean values. In this way the vectors \mathbf{k}_q , besides being orthogonal, are also completely uncorrelated, which improves the identifiability of the model parameters.

For the definition of \mathbf{H} the approach explained below has been adopted. Let $\mathbf{P} = \mathbf{I} - \mathbf{K}(\mathbf{K}^T \mathbf{K})^{-1} \mathbf{K}^T$ be the matrix defining the projection in the space orthogonal to that spanned by \mathbf{K} . This matrix has $N - Q$ eigenvalues equal to one and Q eigenvalues equal to zero [10]. The columns of the matrix \mathbf{H} are then defined as the former. Therefore, since $\mathbf{P} = \mathbf{H}\mathbf{H}^T$, the discrepancy model is built as projection of $\mathcal{GP}(\mathbf{0}, \zeta(\mathbf{X}))$ in the space complementary to the one spanned by the calibration model, so as to avoid confounding between them.

2.2 Covariance functions and hyper parameters

The Equations (7) and (8) (wherein $\delta_{i,j}$ is the Kronecker delta) display the functions $\varrho(\cdot, \cdot)$ and $\zeta(\cdot, \cdot)$, which are represented with square exponential kernels, but parametrised in a similar way as in [8]. A white kernel is also added with respect to the former.

$$\varrho_q(\mathbf{z}_{i,q}, \mathbf{z}_{j,q}) = \frac{1 - \sigma_q^2}{\sigma_q^2} \prod_{p=1}^P \beta_{p,q}^{4(z_{i,p,q} - z_{j,p,q})^2} + \delta_{i,j} \frac{1 - \eta_q^2}{\eta_q^2} \quad (7)$$

$$\zeta(\mathbf{x}_i, \mathbf{x}_j) = \frac{1 - \tau^2}{\tau^2} \prod_{s=1}^S \alpha_s^{4(x_{s,i} - x_{s,j})^2} \quad (8)$$

Such parametrisation has been found convenient because it limits the hyper parameters space to a unit hypercube. In the following the prior probability density distributions adopted for the hyper parameters in Equations (7) and (8) are explained, as well as the underpinning rationales.

For the parameters σ_q^2 , τ^2 , $\beta_{p,q}$ and η_q^2 uniform probability density distributions have been adopted. With respect to the function $\varrho(\cdot, \cdot)$, the hyper parameters σ_q^2 govern the fraction of model output variance captured by the emulator, while the hyper parameters η_q^2 represent explicitly the residual model output variance, due mainly to neglected parameters. Thanks to the property of Automatic Relevance Determination (ARD) [15], naturally possessed by the \mathcal{GP} models, they can easily be traded-off during the optimisation of the emulator, effectively avoiding overfitting. ARD also act on the hyper parameters $\beta_{p,q}$, which will be pushed towards 1 if the respective model parameters have little importance.

The hyper parameters α_s are linked to the boundary conditions (\mathbf{x}_s), of which they measure the correlation with the discrepancy process. In this case, $\mathcal{Beta}(1, 0.1)$ probability density distributions have been chosen in order to strongly aid ARD, and heavily penalise models having \mathbf{x}_s correlated with their discrepancy processes. This set-up is particularly important in order to correctly perform model selection. Indeed, by assuming uninformative prior probability density distributions for these hyper parameters, a highly inadequate model could have a marginal likelihood similar to a more correct one, simply because its discrepancy model yields high likelihood values.

The shape (a) and rate (b) of the gamma probability density distribution used as prior for the simulation precision parameter (λ), were set respectively to 2 and a small value. For practical computational reasons, the latter was defined as the square root of the machine precision times the highest singular value calculated through SVD. These choices had the objectives of yielding a probability density distribution not too informative, while representing the virtually null amount of noise contained in the simulation outputs.

Similarly, the shape (a^*) and rate (b^*) of the gamma prior probability distribution used for the observation precision (λ^*) were set so as to represent the prior information about measurement errors. In particular, $a^* = N \cdot c$ and $b^* = \text{var}(\boldsymbol{\nu}) \cdot N \cdot c$, where $\boldsymbol{\nu}$ are the observation errors, and $c \in [2/N, 1]$. Thus λ^* has mean equal to the precision of the measurement errors, and variance inversely proportional to c , which can be interpreted as the confidence in the information used to determine the extent of these errors.

2.3 Discrepancy analysis

Discrepancy analysis consists of employing the discrepancy model to measure the correlation of each boundary condition (\mathbf{x}_s) with the discrepancy. This correlation is quantified with the generalised correlation coefficient (\mathcal{R}^2) [6]. The significance of a particular \mathbf{x}_s is established by comparing the relative \mathcal{R}^2 index with that corresponding to a fictitious variable \mathbf{x}_0 consisting of Gaussian i.i.d. noise, added in advance to the set of boundary conditions. This comparison is undertaken according to the procedure outlined here below.

For a particular \mathbf{x}_i the relative correlation coefficient \mathcal{R}_i^2 is evaluated as

$$\mathcal{R}_i^2 = \frac{\text{var}[v(\mathbf{X}, \lambda^*, \tau, \alpha_i, \alpha_{j \neq i} = 1)]}{\text{var}(\hat{\mathbf{v}})}$$

where

$$v(\mathbf{X}, \lambda^*, \tau, \alpha_i, \alpha_{j \neq i} = 1) = \mathbf{H}^T \zeta(\mathbf{X}, \mathbf{X}, \tau, \alpha_i, \alpha_{j \neq i} = 1) \mathbf{H} [\mathbf{H}^T (\mathbf{I} \lambda^* + \zeta(\mathbf{X}, \mathbf{X}, \tau, \alpha_i, \alpha_{j \neq i} = 1) \mathbf{H})^{-1} \hat{\mathbf{v}}]$$

i and $j \in [0, s : s = 1, \dots, S]$. In particular, due to the function chosen for $\zeta(\cdot)$, setting $\alpha_{j \neq i} = 1$ makes uninfluential all but the i -th boundary condition. Thus, \mathcal{R}_i^2 represents the fraction of discrepancy variance attributable to \mathbf{x}_i alone, given a particular value of the relative α_i , λ^* and τ . For each \mathcal{R}_i^2 an empirical probability density distribution is inferred from the posterior samples of the α_i , λ^* and τ parameters. Finally estimates and 95% high density intervals (HDI) for the quantity $\tilde{\mathcal{R}}_s^2 = \mathcal{R}_s^2 - \mathcal{R}_0^2$ are calculated. The boundary conditions having 0 lying outside the HDI of their $\tilde{\mathcal{R}}_i^2$ are considered significant in determining the discrepancy between model prediction and field measurements. Significant boundary conditions are ranked according to the respective $\tilde{\mathcal{R}}_i^2$ values.

The interpretation of these results can then be used to upgrade the model, by improving the representation of those processes influenced by significant boundary conditions with high $\tilde{\mathcal{R}}^2$ indexes.

2.4 Model selection

Bayes Factors [12] were adopted as the criteria for performing model comparison and selection. Given the observations \mathbf{y}^* , and two competing models (\mathcal{M}_i and \mathcal{M}_j), the Bayes Factor expressing the evidence supporting \mathcal{M}_j against \mathcal{M}_i ($\mathcal{B}_{j,i}$) corresponds to the ratio between the probability that \mathcal{M}_j generates \mathbf{y}^* and the probability that \mathcal{M}_i generates \mathbf{y}^* :

$$\mathcal{B}_{j,i} = \frac{p(\mathbf{y}^* | \mathcal{M}_j)}{p(\mathbf{y}^* | \mathcal{M}_i)}$$

Table 1: Reference values for Bayes Factor interpretation.

$\log_{10}(\mathcal{B}_{j,i})$	$\mathcal{B}_{j,i}$	Evidence
< 0	< 1	negative
$[0, 1/2]$	$[1, 3.2]$	weak
$[1/2, 1]$	$[3.2, 10]$	substantial
$[1, 2]$	$[10, 100]$	strong
> 2	> 100	decisive

In this case, the probability that the r -th model (\mathcal{M}_r) generates \mathbf{y}^* is proportional to the integral in Equation (9), wherein the subscript r indicates the relation with model \mathcal{M}_r , and \mathcal{S} indicates the space of the parameters listed in its subscript.

$$\begin{aligned}
 L(\mathbf{y}^*|\mathcal{M}_r) = & \\
 & \int_{\mathcal{S}_{\mathbf{z}_r^*, \boldsymbol{\lambda}_r^*}} p(\hat{\mathbf{w}}^*|\mathbf{z}_r^*, \boldsymbol{\lambda}_r^*, \mathcal{M}_r) p(\mathbf{z}_r^*) p(\boldsymbol{\lambda}_r^*) d\mathbf{z}_r^* d\boldsymbol{\lambda}_r^* \times \\
 & \int_{\mathcal{S}_{\boldsymbol{\gamma}_r^*, \lambda_r^*}} p(\hat{\mathbf{v}}|\boldsymbol{\gamma}_r^*, \lambda_r^*) p(\lambda_r^*) p(\boldsymbol{\gamma}_r^*) d\lambda_r^* d\boldsymbol{\gamma}_r^*
 \end{aligned} \tag{9}$$

The quantity $L(\mathbf{y}^*|\mathcal{M}_r)$ (also referred to as marginal likelihood of model \mathcal{M}_r) is usually estimated with Monte Carlo techniques ([23]). In this study Annealed Importance Sampling is used. It is important to notice that, because of the adopted prior probability distributions for the hyper parameters in $\boldsymbol{\gamma}_r^*$, inadequate models with \mathbf{x}_s highly correlated with the discrepancy, will have low $L(\mathbf{y}^*|\mathcal{M}_r)$. Model selection can then be performed according to Table 1.

In order to perform a sensible model comparison it is also advised to follow two sensible rules: (i) to compare models built upon simulation samples of the same size, and (ii) to keep the prior probability density distributions unchanged with respect to rigid translation of the parameter space.

Ideally the model selection process would stop when all the boundary conditions have $\tilde{\mathcal{R}}^2$ indexes not significantly different from zero. However, in real cases this is rarely going to be the case, and the analysis can terminate when the last retained model reaches a sufficient prediction accuracy, as measured by the RMSE. However it is important to highlight that in the presented approach RMSE is not used to performed model selection, which is undertaken according to Bayes Factors, but only as indication of the likely error embedded in the predictions of the retained model.

3 Experiments and results

The test facility (box) is shown in Figure 1, and it had cubic form with internal dimensions $96 \times 96 \times 96$ cm. The roof, floor and walls had all identical, but unknown, composition and thickness of 12 cm. The front wall had a window of dimensions 60×60 cm, wherein the glazed part had an area of 52×52 cm. The whole structure was provided with a support which allowed the influence of the ground to be neglected during the modelling.

The box was used in round robin experiments in the context of IEA Annex 58. In the present paper the focus is on two tests led by the Building Component Energy Test Laboratory (LECE), in Almeria (Spain). The first test (also referred to as ROLBS test) lasted four days (28/06/2013–



Figure 1: The box at the test site.

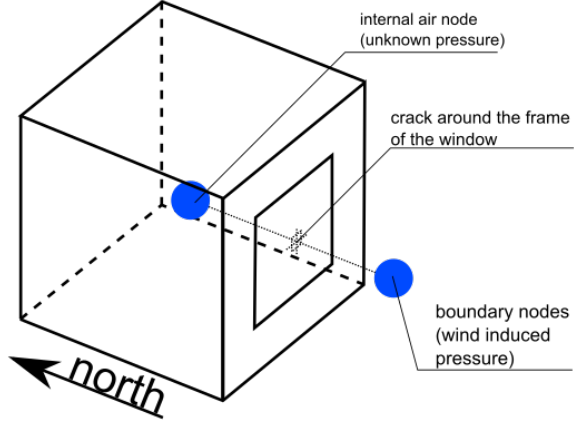


Figure 2: Graphical representation of model \mathcal{M}_3 .

1/07/2013), and consisted of monitoring the internal temperature and the heat flux due to conduction through the walls, while applying a Randomly Ordered Logarithmic Binary Sequence (ROLBS) of heat pulses [22] to the box. In the second test (also referred to as free-float test), the internal temperature was left free to vary, according to the solicitations induced by the weather, and monitored for a period of eight days (02/07/2013–10/07/2013). The boundary conditions were monitored and provided as well. These consisted of: external temperature (Te), global vertical solar radiation of the window plane (Gv), wind speed (Ws), wind direction (Wd) and ROLBS heating pulses (RHP). For more details the reader is referred to [11]. The measurement time step was 1 minute, resulting in time series of 5760 and 11520 observations respectively for the ROLBS and free-float test. Thus, the data were post-processed by bootstrapping the raw time series so as to calculate 15-minutes averages. This allowed a rough estimation of the measurements standard errors, which were used to set-up the observation precision prior probability density distributions.

The calibration experiments undertaken consisted of calibrating a series of six models against the box internal temperature measured during the ROLBS test. These models were created according to the results provided by the discrepancy analysis and their main characteristics are described in the following. The conduction heat flux observed during the ROLBS test, and the internal temperature observed during the free-float test, were used for validation purposes.

Before describing the results of the calibration experiments against the observed internal temperature (real experiments), a series of analogous synthetic experiments, for which the true solution was known and considering only the first three models, is presented in order to prove the capability of the method for identifying suitable upgrades, leading to the more adequate model among the built variants.

Table 2: Parameter prior probability density distributions. x: present in the model, /: not present in the model.

Parameter	Initial value	Distribution	\mathcal{M}_1	\mathcal{M}_2	\mathcal{M}_3	\mathcal{M}_4	\mathcal{M}_5	\mathcal{M}_6
$wall_k$ (W/mK)	NA	$Unif(0.07, 0.13)$	x	/	/	/	/	/
$wall_c$ (kJ/m^3K)	NA	$Unif(1680, 3120)$	x	/	/	/	/	/
$window_t$ (-)	NA	$Uniform(0.5, 0.72)$	/	/	/	x	/	/
$crck1_A$ (mm^2)	790	$Unif(700, 1300)$	/	/	x	/	/	/
$crck2_A$ (mm^2)	NA	$Unif(10, 610)$	/	/	/	/	x	x
$wall_{ext,k}$ (W/mK)	1.05	$Unif(0.7, 1.3)$	/	x	x	x	x	x
$wall1_{ext,c}$ (kJ/m^3K)	3361	$Unif(2240, 4160)$	/	x	x	x	x	/
$wall2_{ext,c}$ (kJ/m^3K)	NA	$Unif(1440, 3360)$	/	/	/	/	/	x
$wall_{ins,k}$ (W/mK)	0.048	$Unif(0.035, 0.065)$	/	x	x	x	x	x
$wall_{ins,c}$ (kJ/m^3K)	179	$Unif(112, 208)$	/	x	x	x	x	x
r/c (-)	0.79	$Unif(0.53, 0.98)$	x	x	x	x	x	x

3.1 Models

Table 2 shows the considered parameters for the different models with the respective prior probability density distributions.

Model \mathcal{M}_1 was built in order to be the simplest representation of the test facility. The box was considered completely sealed (i.e. no air infiltration from the outside was allowed). Since the real composition of the walls was unknown, they were approximated with construction components having only one material layer. The same construction was also used for the window frame. For the glazed component a set of standard fixed property values was assumed. The heating system providing the *RHP* was considered perfect (i.e. with no heat capacity of its own and able to instantaneously transmit the heat to the test box walls and internal air). The set of considered model parameters consisted of: wall conductivity ($wall_k$), wall heat capacity ($wall_c$), and the coefficient determining the fractions of radiative and convective heat provided by the heating system (r/c).

Model \mathcal{M}_2 upgraded \mathcal{M}_1 by substituting the the single material layer construction with one composed of three material layers: two external layers of thickness 3 cm ($wall_{ext}$), made of the same material with high heat capacity and relatively high conductivity, enclosing a third layer of thickness 6 cm ($wall_{ins}$) with low heat capacity and low conductivity. Consequently the conductivities ($wall_{ext,k}$ and $wall_{ins,k}$) and heat capacities ($wall_{ext,c}$ and $wall_{ins,c}$) of the new construction component replaced the conductivity and density of the old one ($wall_k$ and $wall_\rho$).

Model \mathcal{M}_3 was built by adding to \mathcal{M}_2 a component modelling a small crack around the window frame, hypothesising that the window was not perfectly sealed thus allowing the infiltration of air from the outside. The area of the crack was added to the calibration parameter set ($crack1_A$).

Model \mathcal{M}_4 consisted in upgrading \mathcal{M}_2 by better modelling the glazed component and adding the glass optical transmission ($window_t$) to the calibration parameters.

Models \mathcal{M}_5 and \mathcal{M}_6 had the same structure of \mathcal{M}_3 , but the model parameter space was rigidly translated so as to change the ranges of $crack1_A$ and $wall_{ext,c}$. In \mathcal{M}_5 the parameter $crack1_A$ was substituted with $crack2_A$. In \mathcal{M}_6 the parameters $crack1_A$ and $wall_{ext,c}$ were replaced with $crack2_A$ and with $wall2_{ext,c}$ respectively.

3.2 Synthetic Experiments

Model \mathcal{M}_3 was considered as representing the true box, and synthetic observations were generated by running it with parameters set to the initial values displayed in Table 2, and adding white noise to the simulation output according to a noise to variance ratio of 0.01. In this way inadequacies were introduced in models \mathcal{M}_1 and \mathcal{M}_2 , while model \mathcal{M}_3 was free from this kind of errors. These inadequacies were as follows.

Model \mathcal{M}_1 , presented two deficiencies with respect to the true model. Firstly, the lack of heat capacity due to its single layer construction caused a faster transmission of heat provided by *RHP* to the internal air. This made its internal temperature excessively sensitive to the heat pulses. Secondly, due to the absence of wind driven air infiltration from the outside, the internal temperature was less affected by *Te*, *Ws*, and *Wd*.

Model \mathcal{M}_2 , being provided with the correct multi-layer construction, had only the second of the above explained inadequacies.

The plots in Figure 3 show the values of the $\tilde{\mathcal{R}}^2$ indexes of the considered boundary conditions for the three models. The whiskers indicated the 95% high density intervals. With respect to model \mathcal{M}_1 all the boundary conditions were significant. However *Te* and *RHP* appear to have an higher importance, clearly meaning a lack of heat capacity. Similar results were obtained for,

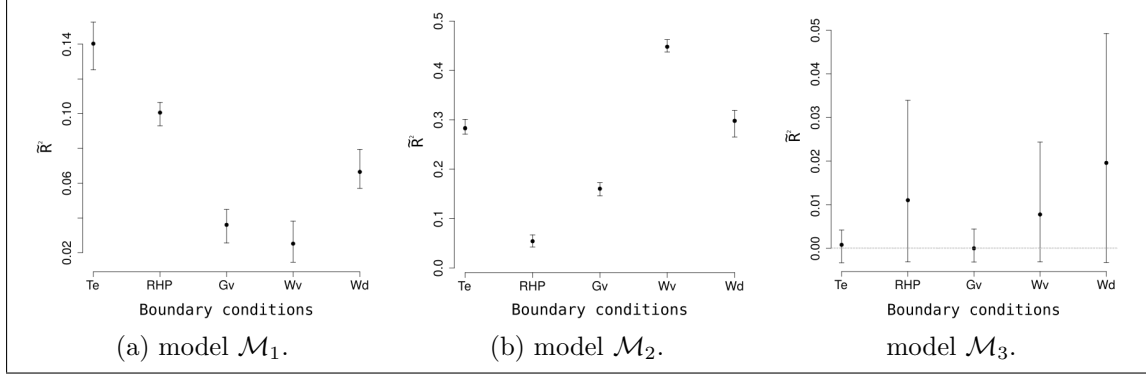


Figure 3: Synthetic experiment: discrepancy analysis results. The whiskers indicate the 95% high density intervals.

Table 3: Synthetic experiments: estimates and 95% HDI for $\log_{10}[L(\mathbf{y}^*|\mathcal{M}_r)]$, and model \mathcal{M}_3 parameters.

(a) $\log_{10}[L(\mathbf{y}^* \mathcal{M}_r)]$.			(b) model \mathcal{M}_3 parameters.		
Model	Estimate	95% HDI	Parameter	Estimate	95% HDI
\mathcal{M}_1	-348.93	[-362.19, -340.40]	$crck1_A$	790	[710, 1200]
\mathcal{M}_2	-52.79	[-62.58, -49.81]	$wall_{ext,k}$	1.21	[0.72, 1.26]
\mathcal{M}_3	812.17	[809.07, 814.38]	$wall1_{ext,c}$	3443	[2880, 4077]
			$wall_{ins,k}$	0.047	[0.041, 0.056]
			$wall_{ins,c}$	163	[117, 202]
			r/c	0.81	[0.66, 0.91]

model \mathcal{M}_2 , but this time Ws and Wd had the highest \tilde{R}^2 , highlighting the possibility of wind driven infiltration. For model \mathcal{M}_3 all the \tilde{R}^2 indexes were not significantly higher than zero, confirming that this model did not have any inadequacy.

The results in Table 3 give further support to the observation just made. Table 3a lists the models' marginal likelihoods, demonstrating that the implemented upgrades, with respect to \mathcal{M}_1 , were decisive improvements ($\mathcal{B}_{2,1} = 296.14$ with $HDI = [278.59, 312.06]$, and $\mathcal{B}_{3,2} = 864.96$ with $HDI = [859.06, 875.37]$). Table 3b contains the estimates and high density intervals (HDI) for the parameters of model \mathcal{M}_3 . Despite minor inaccuracies with respect to weak parameters (e.g. $wall_{ext,k}$ was slightly overestimated), all the variables were accurately inferred.

3.3 Real experiments

Figure 4 summarises the results of the discrepancy analysis driving the creation of the considered models. Table 4 lists the marginal likelihoods and the Bayes factors, while Table 5 contains the RMSEs.

The investigation started by calibrating model \mathcal{M}_1 . The discrepancy analysis provided clear outcomes (Figure 4a) showing that the ROLBS heating pulses were a dominant factor in determining prediction errors, together with the external temperature. This led to the hypothesis that the model was lacking heat capacity. The single-layer construction adopted in \mathcal{M}_1 was substituted with a

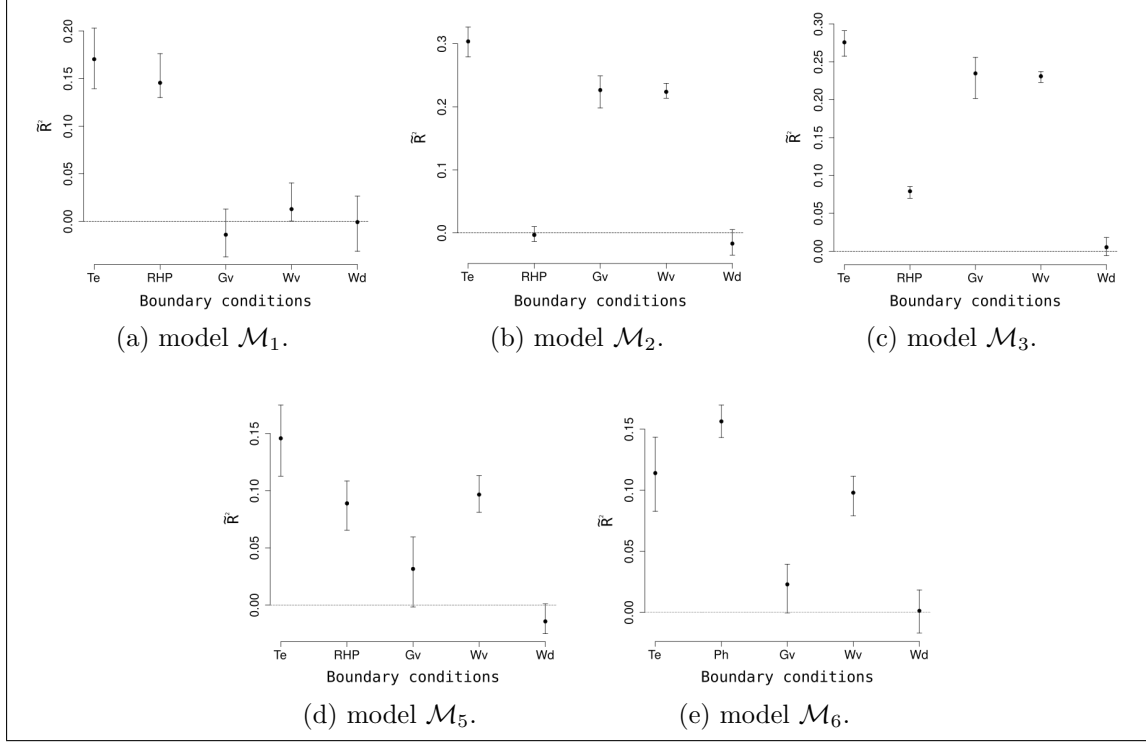


Figure 4: Real experiment: discrepancy analysis results. The whiskers indicate the 95% high density intervals.

multi-layer one, providing for this deficiency, thus creating \mathcal{M}_2 . In particular, the two external layers were able to quickly absorb the induced heat gains, while the central layer was assuring that the walls had the required thermal resistance.

The Bayes Factor $\log_{10}(\mathcal{B}_{2,1})$ was estimated as 619.94 (with HDI = [521.67, 715.92]) showing that the proposed upgrade was decisive. Furthermore the implementation of the multi-layer construction reduced to a negligible level the significance of the *RHP* (Figure 4b). Nonetheless, other boundary conditions, namely *Te*, *Gv* and *Ws*, had \hat{R}^2 indexes significantly different from zero. Thus, two variants of model \mathcal{M}_2 were created. \mathcal{M}_3 tried to address inadequacies caused by *Te* and *Ws*, modelling a little crack around the window frame, thus accounting for wind driven infiltration. \mathcal{M}_4 focused on deficiencies due to a poor processing of *Gv*, by better modelling the glazed component and considering its optical transmission among the calibration parameters.

Both \mathcal{M}_3 and \mathcal{M}_4 did not show enough evidence for being considered significant improvements upon \mathcal{M}_2 . However, $\log_{10}(\mathcal{B}_{3,2})$ on average indicated that the consideration of wind driven infiltration was an important upgrade. Therefore it was decided to refine the modelling of the crack around the window frame, thus creating \mathcal{M}_5 which considered a lower range of values for the area of this feature.

The comparison between \mathcal{M}_5 and \mathcal{M}_2 yielded a Bayes Factor $\log(\mathcal{B}_{5,2})$ equal to 88.83 (with HDI = [54.96, 143.31]), therefore the former was retained as new benchmark model. According

to the relative discrepancy analysis results (Figure 4d) Te , RHP , Ws , were significant. An easy modification was to further adjust the heat capacity of the model so as to address issues related to RHP . In particular, lower values were considered for the heat capacity of the external material layers of the wall construction, thus creating \mathcal{M}_6 .

This last variant had $\log_{10}[L(\mathbf{y}^*|\mathcal{M}_6)]$ equal to 186.77 (with HDI = [178.33, 190.06]), resulting in an additional decisive model improvement ($\log_{10}(\mathcal{B}_{6,5}) = 20.28$, with HDI = [4.36, 44.60]). Nonetheless, the discrepancy analysis returned $\tilde{\mathcal{R}}^2$ qualitatively unvaried with respect to \mathcal{M}_5 . Residual deficiencies were deemed likely to be caused by: (i) the real construction still differing from that implemented; (ii) the neglected heat capacity and heat transmission delay, properties of the real heating system; and (iii) factors such as the pressure coefficients influencing the magnitude of the wind driven infiltration. A better modelling of these aspects was judged impractical due to the lack of the necessary information. Furthermore, \mathcal{M}_6 was deemed to be sufficiently accurate (RMSE = 0.67 C) in predicting the internal temperature of the box during the ROLBS experiment, and overall an adequate representation of the box. Figure 5 displays the obtained fit.

Table 4: Real experiments: estimates and 95% HDI for $\log_{10}[L(\mathbf{y}^*|\mathcal{M}_r)]$ and Bayes factors.

(a) $\log_{10}[L(\mathbf{y}^* \mathcal{M}_r)]$			(b) Bayes factors.		
Model	Estimate	95% HDI	$\mathcal{B}_{i,j}$	Estimate	95% HDI
\mathcal{M}_1	-539.30	[-637.02, -503.83]	$\mathcal{B}_{2,1}$	616.94	[521.67, 715.92]
\mathcal{M}_2	77.64	[26.78, 89.26]	$\mathcal{B}_{3,2}$	44.25	[-14.48, 91.94]
\mathcal{M}_3	121.89	[76.36, 141.00]	$\mathcal{B}_{4,2}$	-42.77	[-83.93, 4.95]
\mathcal{M}_4	34.89	[11.27, 43.58]	$\mathcal{B}_{5,2}$	88.85	[54.96, 143.31]
\mathcal{M}_5	166.50	[145.15, 174.92]	$\mathcal{B}_{6,5}$	20.28	[4.36, 44.60]
\mathcal{M}_6	186.77	[178.33, 190.06]			

Table 5: Real experiments: models' RMSEs against measured internal temperatures.

Model	ROLBS	Free float
\mathcal{M}_1	1.81	1.46
\mathcal{M}_2	1.41	0.84
\mathcal{M}_3	1.35	0.95
\mathcal{M}_4	1.32	0.93
\mathcal{M}_5	1.23	0.93
\mathcal{M}_6	0.67	0.70

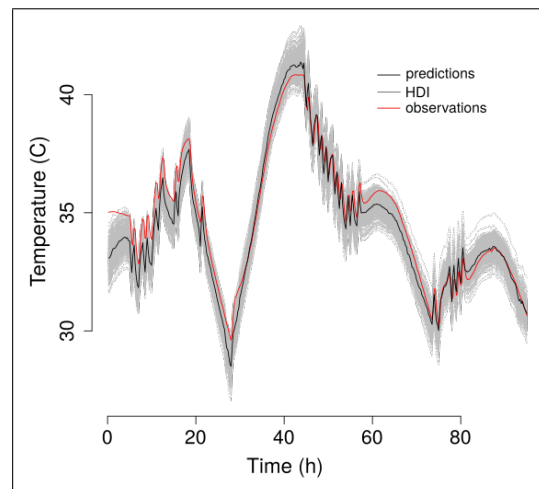


Figure 5: Real experiment: model \mathcal{M}_6 fit. Measurements: red, model predictions: black, prediction 95% HDI: grey.

Table 6: Real and modelled composition of the box walls.

(a) Real composition (from inside to outside).

Layer	Thickness (<i>mm</i>)	Conductivity ($\frac{W}{mK}$)	Heat capacity ($\frac{kJ}{Km^3}$)
fibre cement board 1	36	0.35	1838
xps insulation	60	0.034	36
fibre cement board 1	16	0.35	1838
fibre cement board 2	8	0.60	1960

(b) composition adopted for model \mathcal{M}_6 .

Layer	Thickness (mm)	conductivity ($\frac{W}{mK}$)	Heat capacity ($\frac{kJ}{Km^3}$)
$wall_{ext}$	30	1.24	1891.2
$wall_{ins}$	60	0.052	171
$wall_{ext}$	30	1.24	1891.2

4 Validation

The results obtained from the synthetic experiments demonstrated that the method was able to lead to the progressive identification of the true model, which was correctly characterised by the absence of boundary conditions significantly correlated with the discrepancy. With respect to the real experiments it was observed that the developed models were able to increasingly better predict the box internal temperature (Table 5). However, it was not possible to achieve a model free from inadequacies. Since in this case the true model was unknown, the obtained results were validated utilising data not employed during the calibration, and information disclosed after the undertaken analysis. The former consisted of the conduction heat flux and the internal temperature measured during the ROLBS and free-float experiments respectively. The latter were the real composition of the box walls (Table 6a), and accurate estimates of its Heat Loss Coefficient (HLC) [11].

The HLC, quantifying the heat flowing through the box envelope by conduction for a temperature difference between inside and outside of 1 degree, was estimated through a series of tests in an environmental chamber. Their outcome showed that a sensible range for the HLC was from 3.66 to 4.29 W/K (also referred to as HLC_{EC} values). With respect to the ROLBS test, an analogous estimate equal to 3.64 W/K (also referred to as HLC_{ROLBS} value) was obtained as the ratio between the total measured heat flux and the total measured temperature difference over the test period. The developed computer models were used to estimate these quantities in a Monte Carlo fashion, by sampling the posterior samples inferred for their parameters. The results are displayed in Figure 6a. The obtained empirical probability density distributions were compatible with the range defined by the HLC_{EC} values, especially because the steady-state conditions used in the environmental chamber, consisting in elevated temperature differences across the box envelope (up to 50 C), may have caused an overestimation of the HLC with respect to the real weather conditions. Indeed, the the HLC estimates returned by the developed models gradually approached the HLC_{ROLBS} value, until becoming very similar to it with \mathcal{M}_5 and \mathcal{M}_6 (3.73 and 3.72 W/K respectively).

Similarly, the created models were used to calculate Monte Carlo estimates of the box internal temperature during the free-float test. The Root Mean Squared Errors (RMSEs) between the predicted and measured temperatures are listed in Table 5. As the model was being upgraded, its

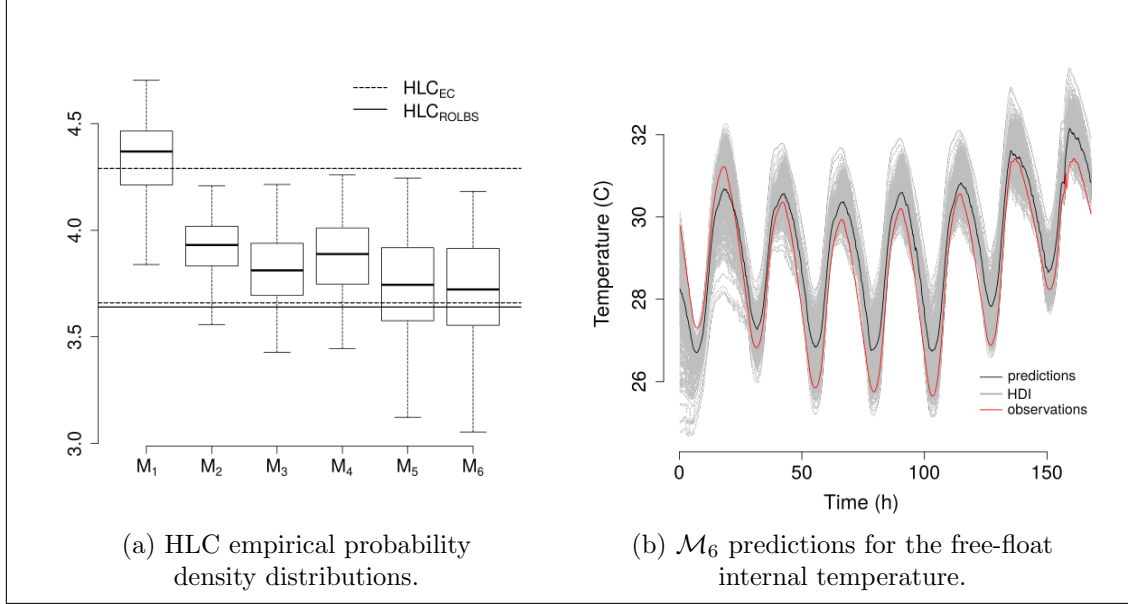


Figure 6: Empirical probability density distribution of HLC obtained through Monte Carlo simulation of the models, and mode \mathcal{M}_6 prediction for the box internal temperature during the free float test.

capability to extrapolate predictions for the free-float conditions improved. Model \mathcal{M}_6 , deemed the best one among the created variants, had the lowest RMSE (0.70 C), and its predictions followed well the box internal temperature observed during the free-float test (Figure 6b).

Furthermore, the modifications applied according to the results provided by the discrepancy analysis resulted in a modelled wall composition qualitatively close to the real one (Table 6). Probably, an adjustment of the conductivity of layer $wall_{ext}$ towards lower values could have additionally improved the model. However, the distributions of thermal capacity and conductivity across the section of the modelled walls appeared a good approximation of the real one.

A final remark is made about the adoption of Bayes Factors as the model selection criterion. The standard practice in the selection of computer models is to use a function of the RMSE as measure of goodness and adequacy of the model. If this same principle had been used for comparing the models developed, it would not have been easy to choose between \mathcal{M}_3 and \mathcal{M}_4 , and probably the latter would have been retained for the marginally lower RMSE (Table 5). However, as the analysis has demonstrated, this would have led to the inclusion of unnecessary parameters such as the glazed component optical transmission, and to a model having an overestimated HLC (Figure 6a). Conversely, Bayes factor were always able to provide clear information about model ranking, overall demonstrating more robustness with respect to model equifinality.

Given these considerations, the proposed approach was considered reliable and able to provide adequate information leading the modelling activity progressively towards a model (\mathcal{M}_6) having properties consistent with the subsequently provided specifications, and capable of extrapolating predictions for boundary conditions different from those considered during its calibration.

5 Conclusions

The paper has presented an approach for the development of computer models with high-dimensional outputs and boundary conditions, aimed at providing adequate support for informed decisions driving the modelling activity, in a similar fashion as in statistical modelling. It consisting of: (i) model calibration in a quasi-Bayesian framework, (ii) the identification of boundary conditions as sources of inadequacy, and (iii) the undertaking of model selection according to Bayes Factors.

The proposed method was demonstrated on synthetic and real experiments, involving building energy models of a test facility employed for round robin tests in the context of the IEA EBC Annex 58. However it is applicable to any models presenting high dimensional outputs and boundary conditions.

The results from the synthetic experiments have demonstrated that the method is able to lead to the correct true model. Ideally, this model is found when no boundary condition shows relevant correlation with the discrepancy between measurements and predictions. For real cases this is rarely going to be the case. Nonetheless, the results obtained against the measured data clearly showed that the procedure is capable of providing useful information about model inadequacies, through the practice called discrepancy analysis. The modeller can use this information to propose consequent model upgrades, according to its domain knowledge. The effectiveness of these upgrades is then evaluated against the evidence provided by the field data. In particular, the adoption of Bayes Factors as the model selection criterion was particularly effective in indicating which model variants were most adequate, leading to a final model of the test facility having properties consistent with specifications provided afterwards the analysis had been undertaken, and able to effectively extrapolate predictions for boundary conditions other than those used in its calibration.

The explained method has been implemented in the open source software Calibro [14], which is being applied and tested, in the context of a major European project [5], on more complex and realistic models.

References

- [1] M. J. Bayarri, J. O. Berger, J. Cafeo, G. Garcia-Donato, F. Liu, J. Palomo, R. J. Parthasarathy, R. Paulo, J. Sacks, and D. Walsh. Computer model validation with functional output. *The Annals of Statistics*, 35(5):1874–1906, Oct 2007.
- [2] M. J. Bayarri, J. O. Berger, D. Higdon, M. C. Kennedy, A. Kottas, R. Paulo, J. Sacks, J. A. Cafeo, J. Cavendish, C. H. Lin, and J. Tu. A framework for validation of computer models. Technical report, National Institute of Statistical Sciences (www.niss.org), 2005.
- [3] M. J. Bayarri, J. O. Berger, M. C. Kennedy, A. Kottas, R. Paulo, J. Sacks, J. A. Cafeo, C. H. Lin, and J. Tu. Bayesian validation of a computer model for vehicle collision. Technical report, National Institute of Statistical Sciences 19 T. W. Alexander Drive PO Box 14006 Research Triangle Park, NC 27709-4006 www.niss.org, 2005.
- [4] Joseph Clarke. *Energy Simulation in Building Design*. Taylor & Francis Ltd, 2001.
- [5] D Costola, J Clarke, N Kelly, and F Monari. A big data approach to the application of building performance simulation to improve the operational performance of large estates. In *Proceedings of Building Simulation 2017: 15th Conference of International Building Performance Simulation Association, San Francisco, 2017*.

- [6] Kjell Doksum and Alexander Samarov. Nonparametric estimation of global functionals and a measure of the explanatory power of covariates in regression. *Ann. Statist.*, 23(5):1443–1473, 10 1995.
- [7] Katrin Heitmann, David Higdon, Charles Nakhleh, and Salman Habib. Cosmic calibration. *Astrophys.J.*, 646:L1–L4, 2006.
- [8] D. Higdon, J. Gattiker, B. Williams, and M. Rightley. Computer model calibration using high-dimensional output. *Journal of the American Statistical Association*, 103(482):570–583, 2008.
- [9] Dave Higdon, Marc Kennedy, James C. Cavendish, John A. Cafeo, and Robert D. Ryne. Combining field data and computer simulations for calibration and prediction. *SIAM Journal on Scientific Computing*, 26(2):448–466, January 2004.
- [10] James S. Hodges and Brian J. Reich. Adding spatially-correlated errors can mess up the fixed effect you love. *The American Statistician*, 64(4):325334, Nov 2010.
- [11] M. J. Jimenez Taboada. Report of subtask 3, part 1: Thermal performance characterization based on full scale testing - description of the common exercises and physical guidelines. Technical report, International Energy Agency, EBC Annex 58, 2016.
- [12] Robert E. Kass and Adrian E. Raftery. Bayes factors. *Journal of the American Statistical Association*, 90(430):773–795, Jun 1995.
- [13] M.C. Kennedy and A. O’Hagan. Bayesian calibration of computer models. *Journal of the Royal Statistical Society, Series B* 63:425–464., 2001.
- [14] F Monari and P A Strachan. Calibro an r package for the automatic calibration of building energy models. In *Proceedings of Building Simulation 2017: 15th Conference of International Building Performance Simulation Association, San Francisco*, 2017.
- [15] Radford M. Neal. *Bayesian Learning for Neural Networks*. PhD thesis, University of Toronto, Secaucus, NJ, USA, 1996.
- [16] RadfordM. Neal. Annealed importance sampling. *Statistics and Computing*, 11(2):125–139, 2001.
- [17] Matthew Plumlee. Bayesian calibration of inexact computer models. *Journal of the American Statistical Association*, 112(519):1274–1285, 2017.
- [18] C.E. Rasmussen and C.K.I. Williams. *Gaussian Process for Machine Learning*. the MIT Press, 2006.
- [19] Mark Strong and Jeremy E. Oakley. When is a model good enough? deriving the expected value of model improvement via specifying internal model discrepancies. *SIAM/ASA Journal on Uncertainty Quantification*, 2(1):106–125, 2014.
- [20] Mark Strong, Jeremy E. Oakley, and Jim Chilcott. Managing structural uncertainty in health economic decision models: a discrepancy approach. *Journal of the Royal Statistical Society: Series C (Applied Statistics)*, 61(1):25–45, 2012.

- [21] Rui Tuo and C. F. Jeff Wu. Efficient calibration for imperfect computer models. *Ann. Statist.*, 43(6):2331–2352, 12 2015.
- [22] HAL van Dijk and FM Tellez. Measurement and data analysis procedures, final report of the joule ii compass project (jou2-ct92-0216). Technical report, 1995.
- [23] V. Vyshemirsky and M.A. Girolami. Bayesian ranking of biochemical system models. *Bioinformatics*, 24(6):833–839, 2008.
- [24] William J. Welch, Robert. J. Buck, Jerome Sacks, Henry P. Wynn, Toby J. Mitchell, and Max D. Morris. Screening, predicting, and computer experiments. *Technometrics*, 34(1):15–25, 1992.